

High-resolution impedance estimation using refraction and reflection FWI constraints: the Fortuna region, offshore Equatorial Guinea

Ian F. Jones^{1*}, Jeet Singh¹, Stuart Greenwood¹, Johnny Chigbo¹, Phil Cox² and Colin Hawke²

Abstract

Seismic imaging and reservoir characterization in the Fortuna region, offshore Equatorial Guinea, is beset with various geophysical challenges related to the presence of extensive, but small-scale low-velocity gas pockets, which give rise to significant and cumulative image distortion at target level. This distortion had not been resolved in a vintage 2013 broadband pre-stack depth migration project, as the velocity model was not sufficiently well resolved, but was subsequently addressed successfully in a project conducted using high-resolution non-parametric tomography with improved broadband deghosted data. The primary objective of that subsequent project was to improve the understanding of the internal structure of the Viscata and Fortuna reservoirs, and this objective was met via clearer internal imaging of these reservoir intervals and the overlying gas-charged sediments. The follow-on work considered here deals with the use of full waveform inversion to further delineate small-scale velocity anomalies associated with the highly compartmentalized reservoir units, and also to use the full waveform inversion velocity model as a constraint during acoustic impedance inversion. We compare the results of impedance inversion using both a conventional approach (with the well-log velocities to build the background trend), with a new approach using a trend derived from high-resolution waveform inversion velocities.

Introduction

The area under consideration lies in deep water offshore Equatorial Guinea, at the frontal toe-thrust zone and frontal deformation zone between the main Niger Delta and NE-SW trending Cameroon volcanic line, comprising a mud-dominated channel levee system deposited in front of a long-lived canyon cut, commonly with post-depositional soft-sediment remobilization in the form of sliding, thrusting and folding. Four wells have been drilled into Fortuna/Viscata formations, although none of these wells were optimally positioned for the Viscata accumulation, as the overlying Fortuna accumulation was the primary objective in all cases. The reservoirs are located in water depths of about 1750 m. The Fortuna reservoir is at about 2550 m sub-sea and seen at 3250 ms two-way time (TWT). The Viscata reservoir is at about 2700 m sub-sea and seen at 3500 ms TWT. The discovered reservoirs are located across two distinct play types:

- Thrust belt: semi-confined turbidite channel systems within structural traps, including the Silenus Hub (Silenus East, Lykos, Estrella de Mar) and Tonel reservoirs
- Forethrust: turbidite channel levee systems with combined structural and stratigraphic trapping mechanisms

The shallower Fortuna reservoir is gas charged and low velocity, which distorts the time structure of the underlying Viscata res-

ervoir, and the extensive nature of these low-velocity anomalies make it impractical to pick them manually, so a robust automated technique was required. This was achieved in a recent depth imaging project (Fruehn et al., 2017), where the primary objective was to obtain a clearer understanding of the internal structure of the Fortuna and Viscata reservoirs. Broadband processing, designed to de-ghost the data, together with high resolution non-parametric tomographic velocity model building and pre-stack depth migration (preSDM) helped to enhance the seismic data for reservoir delineation.

The additional work presented here concerns the estimation of high-resolution velocity fields derived via full waveform inversion (FWI), for use both as interpretation guides and also as constraints for acoustic impedance (AI) inversion. We observe that in a blind well test, the AI results obtained using the FWI velocity constraint provide a better match to the well measurements than do the AI results obtained using a conventional approach.

Multi-azimuth TTI tomographic velocity model-building

The FWI work followed-on from a previous project (Fruehn et al., 2017) wherein six multi-azimuth tomographic model building updates were employed using tilted transversely isotropic (TTI) Kirchhoff and beam migration schemes (Jones, 2010;

¹ ION Geophysical | ² Ophir Energy UK
Corresponding author: ian.jones@iongeo.com
DOI: 10.3997/1365-2397.2018006

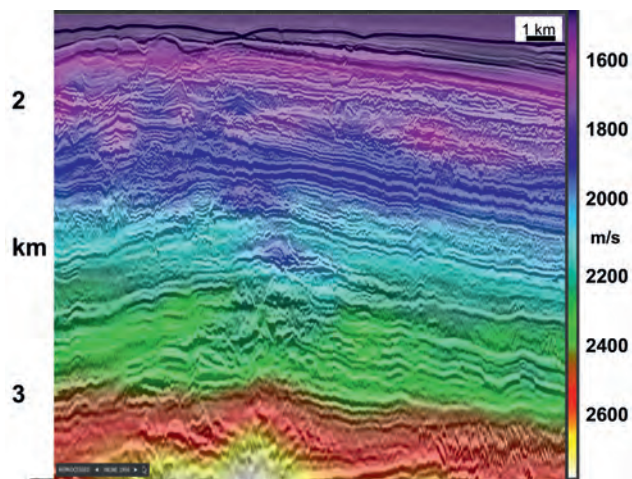


Figure 1 preSDM image with velocity overlay, from the 2016 processing (from Fruehn et al., 2017).

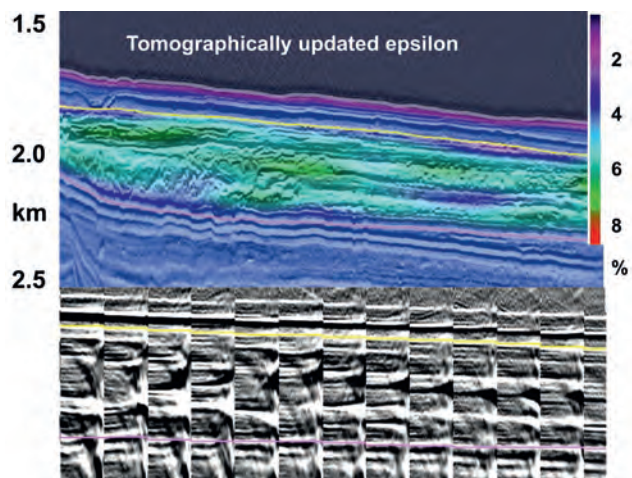


Figure 2 Top: Epsilon model updated via tomographic inversion. Bottom: CRP gathers along the same section of line. Maximum offset is 6 km. (from Fruehn et al., 2017).

2015). This included using wavelet tracking non-parametric move-out picking of offset or angle gathers (Fruehn et al., 2014; Luo et al., 2014) to update velocity and the epsilon anisotropy parameter. Figure 1 shows an inline from the final 3D TTI preSDM image with velocity overlay, and Figure 2 shows the epsilon model and associated (acceptably flat) common reflection-point (CRP) gathers.

At this stage of the model building, where ray-based tomography was used, the velocity model is well suited for imaging, as wavelengths in the model are sufficient to produce a good quality migrated image. The shallower Fortuna reservoir unit is captured in the tomography velocity, as indicated in Figure 3. Vertical resolution of 80 m, delivered by the tomography, is well able to characterize the Fortuna reservoir, which is about 100-m thick, but unable to adequately capture any fine-scale detail in the slightly deeper Viscata reservoir unit.

Input data preparation for FWI

A minimal pre-processing route was adopted for preparing the data for waveform inversion. Only swell noise attenuation and de-bubble were applied. Bandpass filtering was also applied but

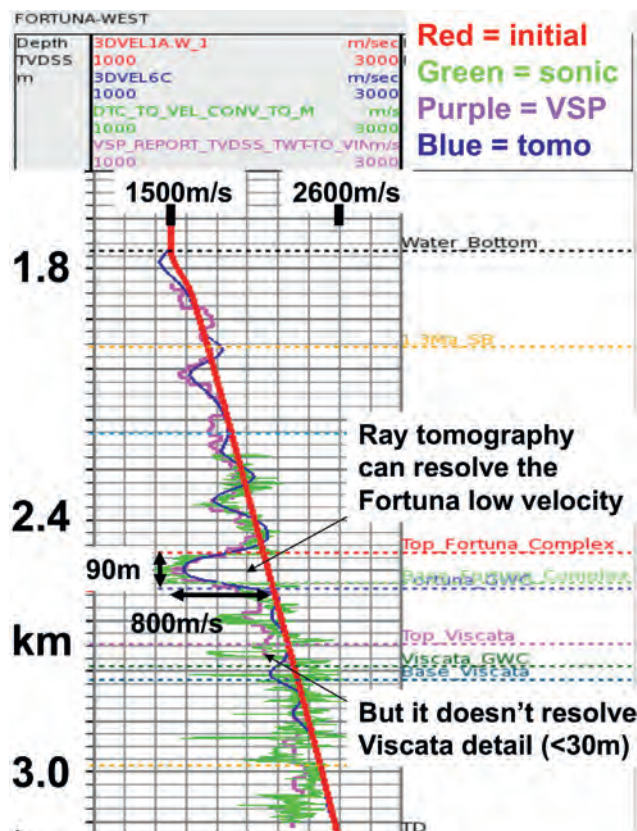


Figure 3 Well log at the Fortuna east location. Green is the sonic, red is the initial model, purple is the VSP, and blue is the tomography model velocity, which is able to capture detail in the Fortuna reservoir with 80 m vertical resolution.

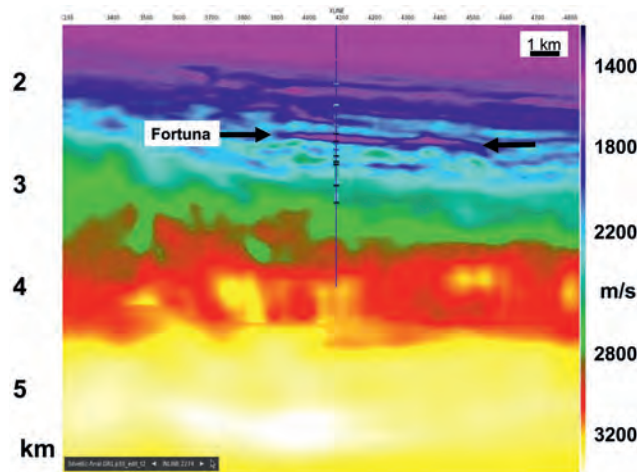


Figure 4 Velocity model derived using several iterations of structurally constrained TTI tomographic inversion: this parameter field was well suited to imaging the complex structure of the reservoir units. The Fortuna reservoir is indicated between the black arrows.

this varied depending on which iteration was being undertaken. Overall, three pass-bands were used during the FWI iterations; namely 1-3-5-9 Hz, 1-3-10-12 Hz, and 1-3-16-20 Hz.

In addition, only the far offsets were used during the early FWI iterations as these relied primarily on refracted arrivals in these deep-water data. Later iterations, when reflections were being used, also utilized the near offset traces. In all cases, the direct wave was muted on input to the inversion.

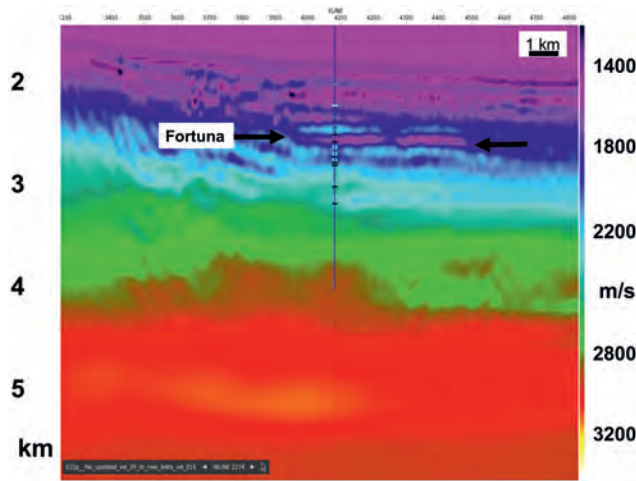


Figure 5 Conventional FWI using the transmitted (refraction) wavefield, within the bandwidth 1-3-5-9 Hz, delineating subtle near-surface velocity variation, and yielding better lateral resolution than ray tomography. The Fortuna reservoir is indicated between the black arrows.

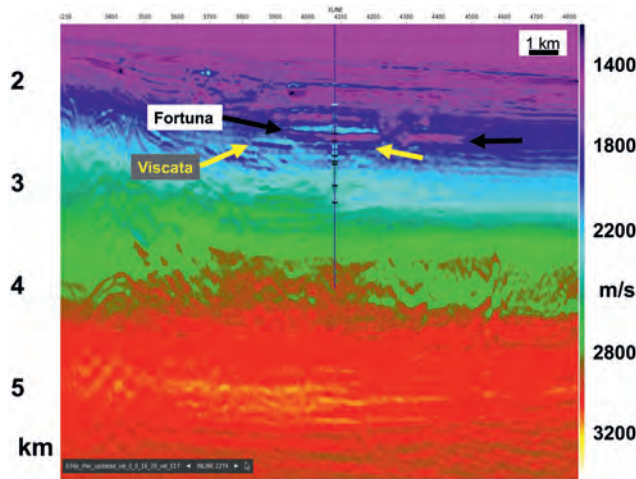


Figure 6 FWI using both the transmitted (refraction) and reflection wavefields, within the bandwidth 1-3-16-20 Hz. The deeper reservoir units at ~2650 m are now well resolved. The deeper Viscata reservoir is now visible as a feature in the velocity model, as denoted by the yellow arrows.

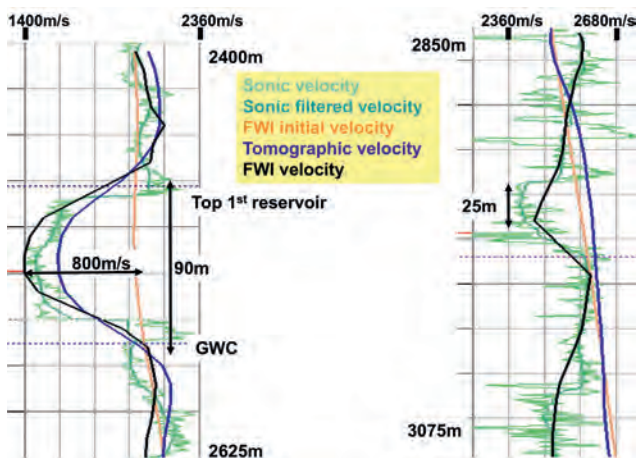


Figure 7 Comparison of FWI results with the well log. Although conventional tomography was able to resolve detail at the level of the Fortuna reservoir (as seen in the enlargement on the left), only the FWI was able to resolve detail at deeper levels, as seen in the segment on the right, showing a better match to the well below the Viscata level.

Waveform inversion

Starting from the structurally constrained TTI tomographic velocity model (Figure 4) after some mild smoothing, several iterations of acoustic refraction FWI were performed, focusing on the far-offsets (Figure 5). This resulted in a significant uplift in the fine-scale structure of the very shallow gas anomaly events near the seabed, but was limited in its vertical reach to around 3 km depth for meaningful velocity update (near the upper reservoir unit). This was to be expected given the maximum available offset of 6 km.

After opening the offset range so as to encompass the full reflection section, subsequent FWI iterations using both refractions and reflections (employing the extended-source reconstructed wavefield method: Wang et al., 2017), resulted in the velocity model shown in Figure 6. The anisotropy parameters were also updated, but only after several iterations of FWI velocity update. Having exploited the reflections, the

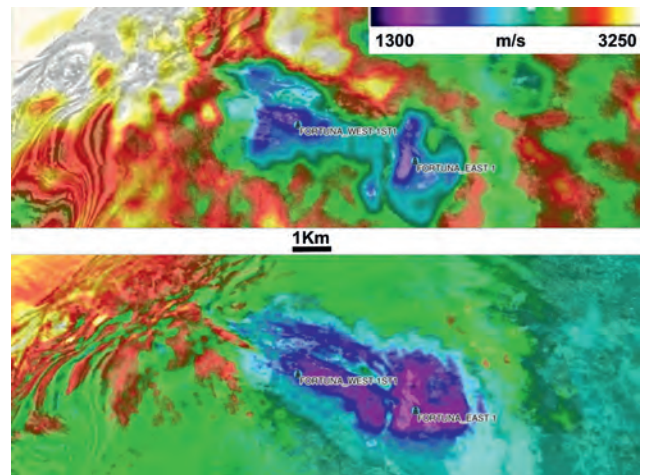


Figure 8 Depth slices through the Fortuna reservoir unit at 2520 m for the tomographic result (top) and the 20 Hz FWI result (bottom).

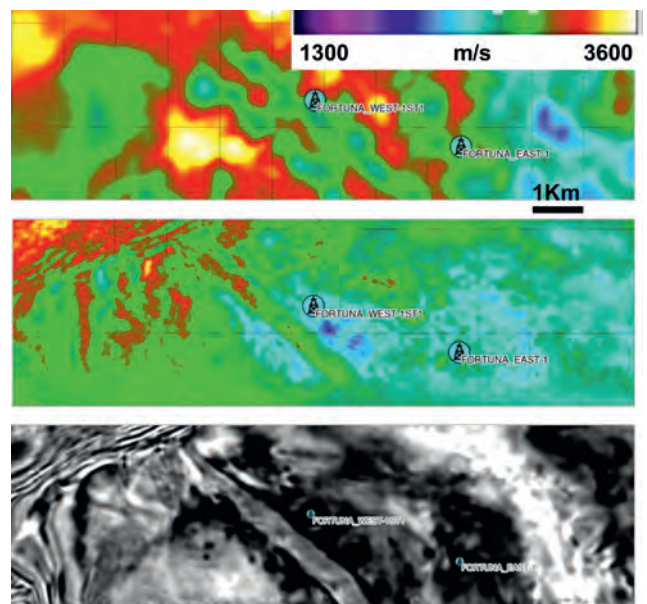


Figure 9 Depth slices through the deeper Viscata reservoir unit at 2650 m for: the tomographic velocity (top) and the 20 Hz FWI velocity (centre), a 60 Hz RTM image (bottom)

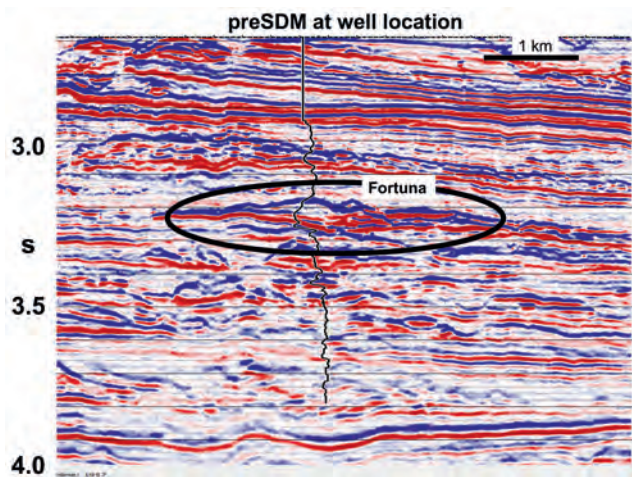


Figure 10 3D TTI preSDM converted to time with Fortuna west well impedance log superimposed. The Fortuna reservoir geobody is indicated.

reach of the meaningful update now extends well below 4 km, giving some new insight into the details of the deeper Viscata reservoir unit.

Whereas the tomographic approach was unable to resolve features in the velocity model much below the level of the Fortuna reservoir, both refraction and reflection FWI were able to extract greater velocity resolution, as shown in the comparison to the well log in Figure 7.

The depth slices through the velocity models near the levels of the Fortuna reservoir (2520 m) and the Viscata reservoir (2650 m) shown in Figures 8 and 9 compare the tomographic and 20 Hz refraction and reflection FWI results, clearly indicating the higher resolution of the velocity field, as expected from a waveform-based approach (Jones et al., 2018).

Using the FWI model for the actual migration resulted in slight improvements to the image and gathers, but its main

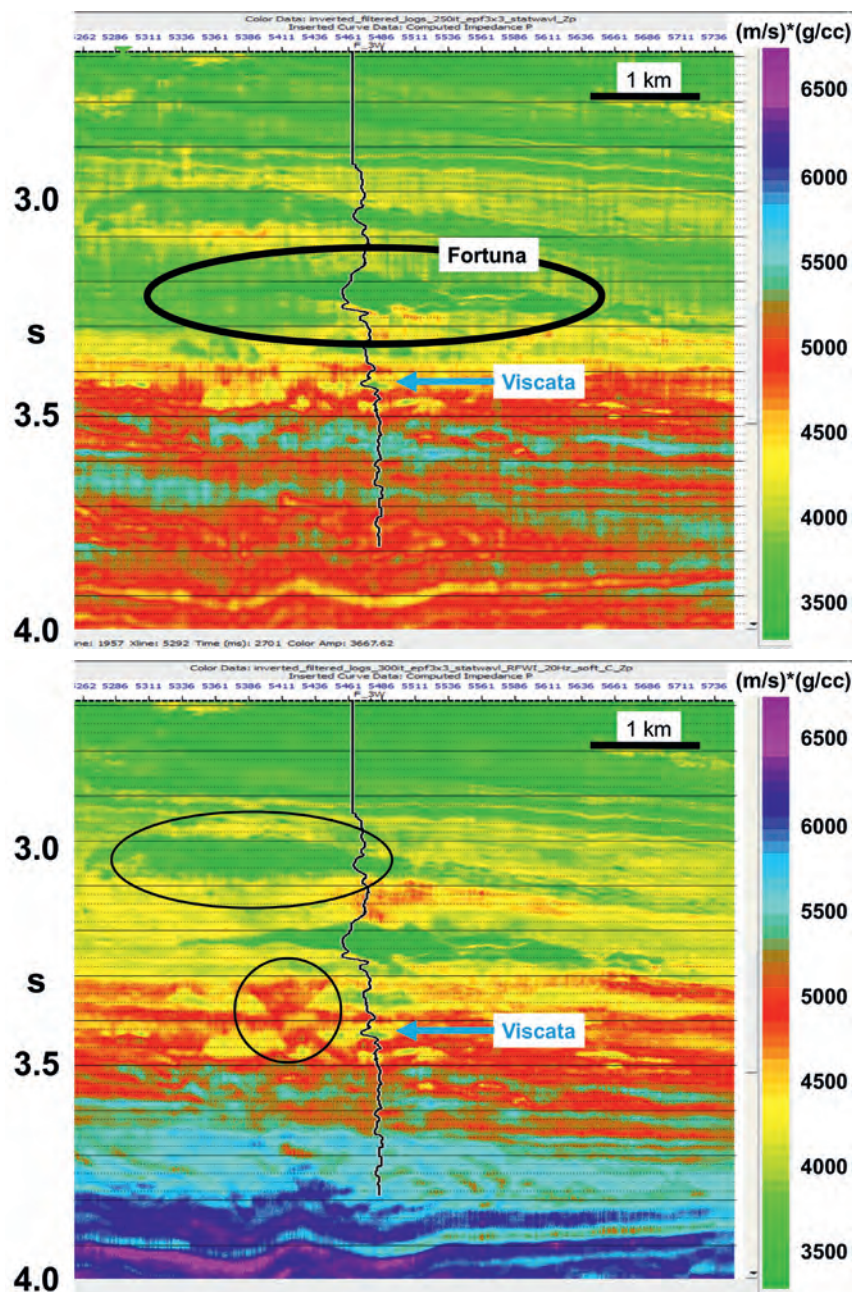


Figure 11 AI inversion results in the vicinity of the Fortuna west well. Top: conventional impedance inversion using the well log sonic and density, constrained by picked horizons. Bottom: impedance inversion using the FWI velocities to create the background low-frequency model with density derived via Gardner's relationship (i.e. no actual well information used). The Fortuna west impedance log is superimposed on both images. An interesting low-AI geobody is now visible at about 3 s on the left of the lower image (encircled) and a channel-cut at the Viscata level is clearly defined (also circled).

interest is in serving to facilitate improvements in acoustic impedance inversion as discussed in the next section.

Acoustic impedance inversion

Conventionally, acoustic impedance (AI) inversion uses the measured well-logged sonic data in conjunction with picked horizon constraints to form a low-frequency background model impedance (LFM). Logged densities can also be used if available; otherwise they can be estimated by using Gardner’s relationship (Gardner et al., 1974).

Here, we first derive a conventional AI result which is obtained using a LFM derived from sonic velocity and density measurements from the well logs and guided by interpreted horizons. These conventional AI results are then compared with an AI inversion obtained without using any well control or picked horizon information at all: namely by simply using the 20 Hz FWI velocities with density derived via Gardner’s

relationship to form the LFM. This approach was previously found to be successful on data from the Gulf of Mexico (Cobo et al., 2018).

Figure 10 shows a section of 3D TTI preSDM image centred on the Fortuna west well, whereas Figure 11 contrasts the AI results using the conventional approach and the FWI constrained method. The FWI result indicated the possibility of a gas accumulation at about 3 s TWT, to the left of the well location (circled), and also gives a clearer indication of a channel-cut at the Viscata reservoir level (encircled). The perspective view shown in Figure 12 shows this more clearly.

Figure 13 shows the AI computed from well log sonic velocity and density compared to the AI results extracted at the well location from the conventional approach and with the FWI method. As expected at the well location, where the well was

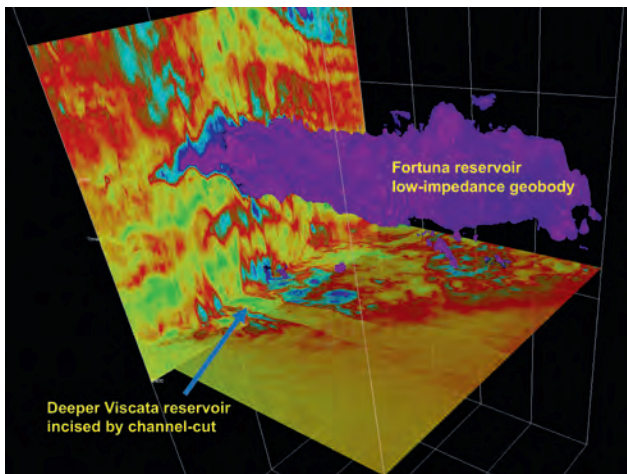


Figure 12 3D perspective view of post stack acoustic impedance results in the vicinity of the Fortuna west well, with depth slice highlighting the channel-cut through the region of the Viscata reservoir.

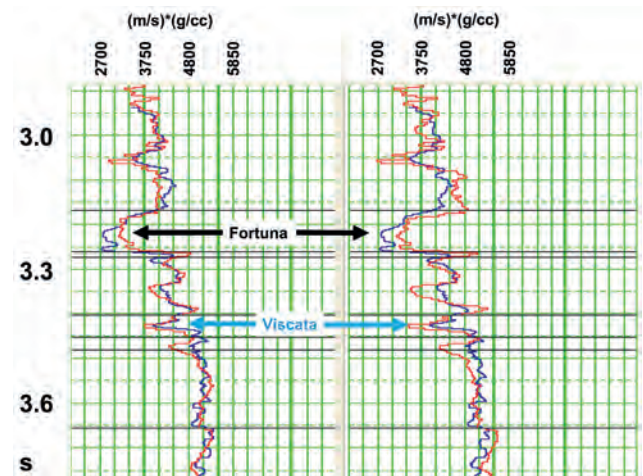


Figure 13 Post-stack acoustic impedance results for the Fortuna west well. The well impedance is shown in blue. Left: conventional approach using the well-log trend in conjunction with interpreted horizons and density from the actual density log (red curve). Right: using the FWI velocity model to create the LFM, with density derived via Gardner’s relationship i.e. no actual well information, or interpretation, used (red curve).

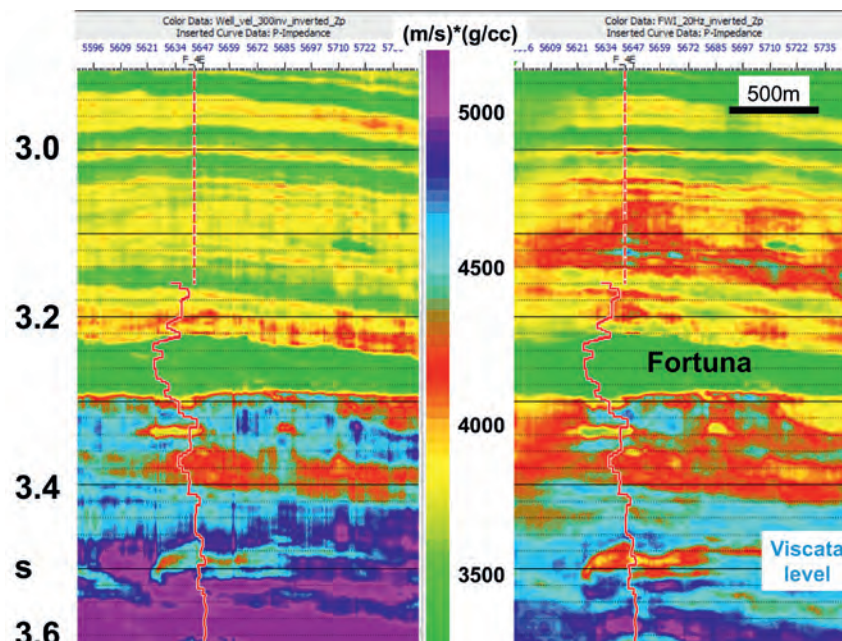


Figure 14 Blind-test AI inversion results in the vicinity of the Fortuna east well. Left: conventional impedance inversion (using the Fortuna west well as its constraint). Right: impedance inversion using the FWI velocities to create the background low-frequency model. The Fortuna east impedance log superimposed on both images.

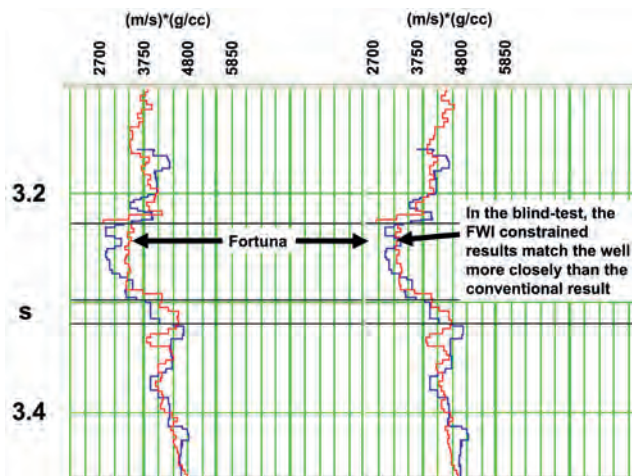


Figure 15 Blind-test AI results compared to the Fortuna east well over the main reservoir interval. The well impedance is shown in blue. Left: AI obtained using the conventional approach with the Fortuna west well sonic and density as its constraint (red curve). Right: AI obtained using the FWI velocity model as the LFM, with density derived via Gardner's relationship (red curve). The FWI results match the log much more closely in the vicinity of the low-impedance Fortuna reservoir interval.

the constraint, the conventional result shows a very good match (slightly better than that of the FWI approach). But the FWI AI result, which is very similar, was created without using any external independent constraints for building the LFM, i.e. no well log information and no interpreted horizons which can suffer from potential interpretational bias.

Blind test results

The conventional approach used the Fortuna west well as its constraint, but we also had a second well to the east, and this was used to conduct a blind test of both AI inversion results. In this case, the FWI approach outperforms the conventional approach: Figure 14 compares the 'blind' AI results with the Fortuna east well superimposed, and Figure 15 shows computed log AI contrasted with the AI profiles at the east well location.

Conclusions

Detailed imaging of the internal reservoir structure of the Viscata and Fortuna fields has been achieved using a velocity model derived from several iterations of ray-based tomographic inversion, using structural constraints and non-parametric moveout picking. In addition, a velocity model obtained using 20 Hz FWI was derived to serve as an interpretational guide. This model delivered slight improvements to the image and gathers, but its main interest is in serving to facilitate improvements in acoustic impedance inversion as compared to the more conventional approach of using well logs to furnish the LFM as the constraint. In the method presented here, no

well-log information was employed in the AI inversion, and no interpreted horizons (which can introduce bias) were required to build the LFM.

In the blind test results, the new approach to AI inversion using constraints from FWI velocities produces a significantly better match with the well data at the Fortuna reservoir level. In addition to facilitating improved imaging, this indicates a very useful application for the parameter fields derived from FWI, whether that be for better pore pressure prediction using the high-resolution velocities, or for impedance inversion, as shown here.

Acknowledgements

We would like to thank the Ophir partnership for permission to present this work, and Ion Geophysical for permission to present the processing technology, and to John Brittan, Jacques Leveille, Carlos Calderon, Peter Rowbotham, and the journal reviewer for their helpful editorial suggestions.

References

- Cobo, Y., Chi., S. and Calderon-Macias, C. [2018]. Quantitative interpretation from full-waveform inversion in a deep water GOM dataset. *80th annual meeting of the European Association of Exploration Geophysicists*, Abstracts.
- Fruehn, J.K., Greenwood, S., Valler, V. and Sekulic, D. [2014]. Resolving small-scale near-seabed velocity anomalies using non-parametric autopicking and hybrid tomography. *CSEG Recorder*, **39** (10), 28-33.
- Fruehn, J.K., Harger, D., Cox, P., Minifie, D., Chigbo, J. and Smith, M. [2017]. Imaging buried channel systems under a complex overburden: the Fortuna region, offshore Equatorial Guinea. *PESGB Africa Workshop*, Abstracts.
- Gardner, G.H.F., Gardner, L.W. and Gregory, A.R. [1974]. Formation velocity and density - The diagnostic basics for stratigraphic traps. *Geophysics*, **39**, 770-780.
- Jones, I.F., Singh, J., Cox, P., Warner, M., Hawke, C., Harger, D. and Greenwood, S. [2018]. High resolution impedance estimation using refraction and reflection FWI: the Fortuna region, offshore Equatorial Guinea. *1st EAGE-PESGB velocities workshop*, Abstracts.
- Jones, I.F. [2015]. Estimating subsurface parameter fields for seismic migration: velocity model building. In: Grechka, V. and Wapenaar, K. (Eds.) *Encyclopedia of Exploration Geophysics*. SEG, U1-1-U1-24.
- Jones, I.F. [2010]. *An introduction to velocity model building*. EAGE, Houten, The Netherlands.
- Luo Z., Brittan, J., Fan, D., Mecham, B., Farmer, P. and Martin, G. [2014]. Imaging complexity in the earth — Case studies with optimized ray tomography. *The Leading Edge*, **33** (9), 1016-1022.
- Wang, C., Yingst, D., Farmer, P., Jones, I., Martin, G. and Leveille, J. [2017]. Reconstructed full-waveform inversion with the extended source. *87th SEG Annual Meeting*, Expanded Abstracts, FW15.1.